Bioinformatics, YYYY, 0–0
doi: 10.1093/bioinformatics/xxxxx
Advance Access Publication Date: DD Month YYYY
Manuscript Category

Subject Section

CLPred: A sequence-based protein crystallization predictor using BLSTM neural network

Wenjing Xuan[1,2], Ning Liu[1], Neng Huang[1], Yaohang Li[3,*], Jianxin Wang[1,2,*]

[1]School of Computer Science and Engineering, Central South University, Changsha, 410083, China

[2]Hunan Provincial Key Lab on Bioinformatics, Central South University, Changsha, 410083, China

[3]Department of Computer Science, Old Dominion University, Norfolk, 23529, Virginia, United States

*To whom correspondence should be addressed.

Abstract

Motivation: Determining the structures of proteins is a critical step to understand their biological functions. Crystallography-based X-ray diffraction technique is the main method for experimental protein structure determination. However, the underlying crystallization process, which needs multiple time-consuming and costly experimental steps, has a high attrition rate. To overcome this issue, a series of *in-silico* methods have been developed with the primary aim of selecting the protein sequences that are promising to be crystallized. However, the predictive performance of the current methods is modest.

Results: We propose a deep learning model, so-called CLPred, which uses a bidirectional recurrent neural network with long short-term memory (BLSTM) to capture the long-range interaction patterns between *k*-mers amino acids to predict protein crystallizability. Using sequence only information, CLPred outperforms the existing deep-learning predictors and a vast majority of sequence-based diffraction-quality crystals predictors on three independent test sets. The results highlight the effectiveness of BLSTM in capturing non-local, long-range inter-peptide interaction patterns to distinguish proteins that can result in diffraction-quality crystals from those that cannot. CLPred has been steadily improved over the previous window-based neural networks, which is able to predict crystallization propensity with high accuracy. CLPred can also be improved significantly if it incorporates additional features from pre-extracted evolutional, structural, and physicochemical characteristics. The correctness of CLPred predictions is further validated by the case studies of Sox transcription factor family member proteins and Zika virus non-structural proteins.

Availability: https://github.com/xuanwenjing/CLPred

Contact: jxwang@mail.csu.edu.cn; yaohang@cs.odu.edu

1 Introduction

Protein crystallography is increasingly favored by the majority of researchers because protein structure analysis is the basis of protein functional research (Bethel and Lieberman, 2014), disease treatment (Xue *et al.*, 2013), and drug design (Cordeiro and Speck-Planche, 2012; Chen and Yu, 2013). At present, about 80%~90% of the known protein three-dimensional structures are obtained using X-ray diffraction (XRD) analysis technology. XRD determines the three-dimensional coordinates of heavy atoms in protein molecules within certain resolution by measuring the spatial distribution of electron density in protein crystals. To determine the 3D structures of proteins by XRD, forming protein crystals suitable for structural analysis is crucial. The experimental process of obtaining protein crystals consists of multiple costly and time-consuming steps, including selection, cloning, expression, purification, and crystallization. Over 60% of the structure determination costs are consumed by unsuccessful attempts (Service, 2005; Kurgan and Mizianty, 2009). Only ~2-10% of protein targets produce high-resolution protein structures (Slabinski *et al.*, 2007) and ~4.6% of targets produce diffraction-quality crystals (Jahandideh *et al.*, 2014). Crystallization is characterized by a significant rate of attrition and is among the most complex but poorly understood problems in structural biology (Kurgan and Mizianty, 2009), which provides motivation for further research of this field. Researchers consider the intrinsic factor that affects the success rate of protein crystallization is the crystallinity of the protein itself (Sánchez-Puig *et al.*, 2012). If there is a prediction method that can predict the crystallinity of a protein with satisfactory accuracy, it will enable rapid *in-silico* screening target proteins that are predicted to have lower crystallization propensity, and consequently, trial-and-error settings and costs of protein structure analysis will be significantly reduced. Several investigations suggested that the features derived from protein sequences could be used for predicting crystallization propensity (Canaves *et al.*, 2004; Goh *et al.*, 2004). Therefore, it is of a great need to develop highly accurate *in-silico* methods to distinguish proteins that can lead to diffraction-quality crystals from those that cannot, based on their sequences and characteristics before crystallization experiments.

In recent years, a series of prediction models and statistical methods for protein crystallization propensity, which use sequence-derived or secondary structural properties, have been developed. CrystalP2 (Kurgan *et al.*, 2009) breaks the limitation of its predecessor version CrystalP (Chen *et al.*, 2007) to predict only short-chain proteins. It is a kernel-based method that considers a large number of input features including composition and collocation of amino acids (AAs), pI, and hydrophobicity. PPCpred (Mizianty and Kurgan, 2011), based on a Support Vector Machine (SVM) model, is the first one by integrating sequence-derived features with structural features to predict protein production, purification, crystallization, and production of diffraction-quality crystals as the four-stop states. Inspired by PPCpred, a two-layer SVM predictor PredPPCrys (Wang *et al.*, 2014) is developed by using a set of comprehensive and multifaceted sequence-derived features, which has better prediction performance than the single-layer SVM. XtalPred–RF (Jahandideh, *et al.*, 2014) improves XtalPred (Slabinski *et al.*, 2007) by using a simple statistical analysis of the physicochemical features of a protein and then applying a random forest model to select additional features, such as predicted surface ruggedness, hydrophobicity, side-chain entropy of surface residues, and amino acid composition of the predicted protein surface. TargetCrys (Hu *et al.*, 2016) is a two-layer SVM predictor that takes advantage of multi-view protein features. Crysf (Wang *et al.*, 2018) exploits the UniProt-derived functional annotations to predict the crystallization propensity of proteins, but its performance is limited by the proteins available in UniProt. fDETECT (Meng *et al.*, 2017) employs the logistic regression model to predict four-stop states with the advantages of less computational time and more accuracy. The majority of these tools perform a two-stage classification using a plethora of sequence-based features: i). performing feature selection and engineering using additional tools; and ii). feeding the selected features to the machine learning algorithms for classification. These computational methods and tools not only lead to performance improvement, but also promote the understanding of protein crystallization.

In recent years, deep learning makes significant contributions to the field of bioinformatics. Recent work (Elbasir *et al.*, 2019) shows that using deep learning to extract features often achieves better results compared to its closest machine learning competitors. The majority of these deep learning algorithms rely on features extracted from raw sequences. The study (Elbasir *et al.*, 2019) builds a convolutional neural network (CNN) (LeCun *et al.*, 1998) to extract features such as frequency sets of amino acid *k*-mers and *k*-mers information. Studies in protein secondary structure show that the types of neighboring residues play a predominant role in the secondary structure conformation that a residue adopts. In particular, residues in contacting parallel or antiparallel β-sheets are connected by hydrogen bonds in alternative positions. The hydrogen bonds between residues at positions *i* and *i*+3, *i* and *i*+4, and *i* and *i*+5 lead to the formation of 3-10 helices, α-helices, and π-helices, respectively (Li *et al.*, 2011). Certain *k*-mers form structural keywords that can effectively distinguish between major protein folds (Elhefnawy *et al.*, 2019). CNN can often effectively capture such local motif patterns between interactions of *k*-mers, but have difficulty in learning high-order, long-range interactions of *k*-mers, which are essential to form stable spatial structures. Mining the long-range peptide-peptide interactions in proteins (i.e., non-local, remote interactions between *k*-mers) is critical to solve the riddle of protein crystallization propensity prediction.

In this study, we build a deep learning network to extract global interaction patterns, improving over the traditional window-based neural network. CNN is a feed-forward neural network, which can effectively capture non-linear spatial information in image classification and other computer vision problems (Szegedy *et al.*, 2015). Moreover, it has also achieved promising results in many natural language processing (NLP) tasks. CNN is often used to capture local patterns, but have difficulty in learning long-range interactions information. In contrast, recurrent neural network (RNN) is usually effective in solving this problem. Long Short-Term Memory (LSTM) (Hochreiter and Schmidhuber, 1997) is a special RNN designed to address vanishing gradient problem, so that the network is able to learn over hundreds of time steps. LSTM has a designed memory sub-architecture called 'memory cell' to store non-decaying information, which is realized by volume-conserving mappings constructed through a linear unit with a weight one self-recurrent connection. It performs well in machine translation (Sutskever *et al.*, 2014) and speech recognition (Graves and Jaitly, 2014) as well as the prediction of protein secondary structure based on protein sequence (Sønderby and Winther, 2014).

In this paper, we propose CLPred, a deep learning framework protein crystallization prediction only based on sequence information. It first takes a raw protein sequence as input and converts the amino acids into word vector representation through a word embedding layer. Then the word vectors are passed to a CNN layer whose goal is to capture the high-frequency *k*-mers features. Finally, the *k*-mers features are supplied to an LSTM layer, which uses feed-forward neural networks for concatenation of predictions from the forward and backward networks in the bidirectional model to capture the long-range interactions information between *k*-mers amino acids and generate predictions. The key amino acids and tripeptides influencing protein crystallization are obtained by analyzing the feature vectors. CLPred can be improved significantly if it incorporates additional features. In addition, the correctness of our CLPred predictions is further validated by the case studies of Sox transcription factor family member proteins and Zika virus non-structural proteins.

Table 1. Statistics for training and testing sets.

Dataset	No.of crystallizable	No.of uncrystallizable	Total
Training set (Elbasiret al., 2019)	4420	22401	26821
DC_final (Elbasiret al., 2019)	891	896	1787
SP_final (Elbasiret al., 2020)	148	89	237
TR_final (Elbasiret al., 2020)	374	638	1012

2 Materials and methods

2.1 Data preparation

We use four data sets in this work, including a training set and three test sets. The training set and one of the test sets are obtained from DeepCrystal (Elbasir *et al.*, 2019). It was originally generated by (Wang *et al.*, 2014), including five categories: diffraction-quality crystal, protein cloning failure, protein material production failure, purification failure, and crystallization failure. In Elbasir *et al.* (2019), diffraction-quality crystal is treated as a positive class and the remaining four are combined as a single negative class. Then it exploits the CD-HIT (Fu *et al.*, 2012) method to remove sequences from the training set which have over 25% sequence identity with the test set. For sequences with length less than 800, zero padding is applied to make all input sequences have equal lengths of 800. Finally, the data set is randomly divided into two disjoint parts: a training set with 26,821 sequences (4,420 crystallizable and 22,401 non-crystallizable) and a test set with 1,787 sequences (891 crystallizable and 896 non-crystallizable). We also remove sequences from the training set with over 25% sequence identity to Sox9, Sox17, and Zika proteins for our case studies. We name the test set 'DC_final' since it is obtained from DeepCrystal.

In addition, we adopt two other independent test sets named 'SP_final' and 'TR_final' from BCrystal (Elbasir *et al.*, 2020) for further verification. These two test sets are first extracted from 'SP_test_nr' and 'TR_test_nr' (Wang *et al.*, 2018), which have 604 and 2,521 protein sequences, respectively. Since 'SP_test_nr' and 'TR_test_nr' are derived from TargetTrack (Kouranov *et al.*, 2006), they may overlap with the training set. Elbasir *et al.* (2020) use CD-HIT method to remove sequences from 'SP_test_nr' and 'TR_test_nr' with over 25% sequence identity to the training set. Sequences with length over 800 are also removed. The post-processed 'SP_test_nr' and 'TR_test_nr' datasets are named 'SP_final' and 'TR_final', respectively. Moreover, we remove the N-terminal hexaHis tag (MGHHHHHHSH) and the C-terminal LEHHHHHH tag presented in some sequences. These tags are not part of the original protein sequences, but are added artificially to ease purification (Gräslund *et al.*, 2008). Detailed statistics information of the above four data sets is listed in Table 1.

2.2 Model architecture

The protein crystallization prediction is a binary classification problem. For an input protein sequence, the corresponding crystallization score in range [0, 1] is predicted. As shown in Fig. 1, CLPred obtains the raw sequence from input, transforms *k*-mers amino acids into word vector representation through the embedding layer, then respectively extracts high-frequency *k*-mers features and long-range interaction features through CNN and BLSTM layers, and thus completes end-to-end protein diffraction-quality crystals prediction. Our model architecture including features embedding and various layers are described next.

The embedding layer in CLPred transforms the discrete amino acid sequence encoding into a dense, continuous vector representation. Compared to the one-hot representation, which is sparse, the embedding layer has the advantage of dimension reduction while preserving the important physicochemical properties of amino acids in a protein sequence (Vang and Xie, 2017). In the embedding layer, the input of a protein sequence is encoded as $X = (x_1, x_2, \dots, x_L), x_i \in \{0, 1, \dots, 21\}$, where 1 to 20 represent the types of amino acids in alphabet order, gaps are filled with 0s, ambiguous or unknown amino acids are denoted as 21, and $L = 800$ is the fixed length. The embedding algorithm learns a feature matrix, which is denoted by $W_e \in \mathbb{R}^{22\times 50}$, where 22 is the number of input types and 50 is the embedding dimension. The matrix represents the dense representation of each amino acid. W_e is initialized randomly and trained along with the whole network. By looking up W_e , the embedding layer outputs a feature map $F_e \in \mathbb{R}^{L\times 50}$.

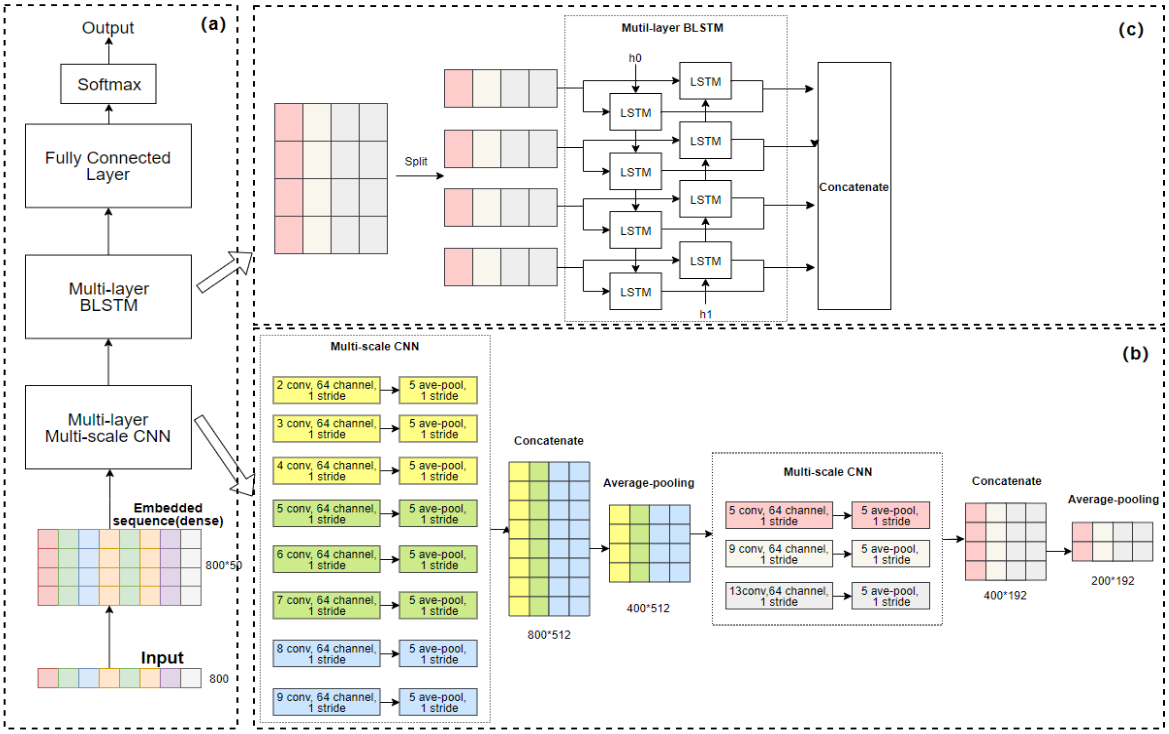
(a)
Output
Softmax
Fully Connected Layer
Multi-layer BLSTM
Multi-layer Multi-scale CNN
Embedded sequence(dense)
800*50
Input
800
(c)
Mutil-layer BLSTM
h0
LSTM
h1
Split
Concatenate
(b)
Multi-scale CNN
2 conv, 64 channel, 1 stride
3 conv, 64 channel, 1 stride
4 conv, 64 channel, 1 stride
5 conv, 64 channel, 1 stride
6 conv, 64 channel, 1 stride
7 conv, 64 channel, 1 stride
8 conv, 64 channel, 1 stride
9 conv, 64 channel, 1 stride
5 ave-pool, 1 stride
Concatenate
800*512
Average-pooling
400*512
Multi-scale CNN
5 conv, 64 channel, 1 stride
9 conv, 64 channel, 1 stride
13conv,64 channel, 1 stride
5 ave-pool, 1 stride
Concatenate
400*192
Average-pooling
200*192

Fig. 1. The architecture of CLPred. (a). The overall workflow of CLPred. (b). The architecture of the CNN module. (c) BLSTM module. The discrete raw sequence is transformed into a dense, continuous vector through feature embedding and then fed into the CNN layer with multi-scale convolution kernels to capture local amino acid *k*-mers features. The extracted characteristic map of the CNN layer is passed to BLSTM concatenating the forward and backward information to capture the long-range interaction characteristics between *k*-mers. Finally, all the BLSTM outputs are passed to the fully connected layers to produce protein crystal prediction scores.

After the embedding layer, the protein sequence is encoded into a dense, continuous vector representation F_e and fed to the CNN layer. Inspired by previous work (Elbasir *et al.*, 2019), we construct a multi-layer multi-scale one-dimensional convolution module but with certain adjustments. Our convolution module consists of two CNN layers. The first CNN layer contains 8 kernels as shown in Fig. 1(b). The variational size of the convolution filter is designed to capture *k*-mers amino acid fragments, where *k* ranges from 2 (a dipeptide) to 9 (a nonapeptide). The second layer is composed of 3 kernels, which is represented as $\{K_j^n\}_{n=1,2,3,j=5,9,13}$, where *n* is the *n*th kernels and *j* is the corresponding kernel size. The kernel size is equal to the size of a convolutional window across *j* characters and the parameters are tuned according to training and validation. An intermediate feature map F_m^i in CNN layer with respect to the *i*th kernel is extracted as

$$F_m^i = ReLU\left(Conv(F_e, K^i)\right),$$

where *ReLU* is the rectified linear unit activation function and *Conv* denotes the convolution operation (Nair and Hinton, 2010; Krizhevsky *et al.*, 2012; LeCun *et al.*, 2015).

After obtaining an intermediate convolution feature map F_m^i, average pooling operation is used to down-sample the latent representation by taking the average value over the sub-regions of the CNN layer outputs, which is helpful to maintain the integrity of information and facilitate the subsequent extraction of global features. After average pooling, the outputs from all the kernels are concatenated for another average pooling operation to generate the feature map F_c for the next layer. The overall generation of the feature map F_c is formulated as follows:

$$F_c = AvgPooling(Concat(AvgPooling(F_m^i))),$$

where *AvgPooling* and *Concat* are the average pooling and the concatenation operations, respectively.

A multi-layer Bidirectional LSTM (BLSTM) module is designed following the CNN and pooling layers, as shown in Fig. 1(c). CLPred has 3 BLSTM layers. Each direction in the BLSTM consists of 200 time step nodes while each time step is composed of 128 hidden units. Fully connected neurons in the network are activated by ReLU. We adopt 0.5 dropout rates to prevent overfitting and co-adaptation (Hinton *et al.*, 2012). The BLSTM layer $h_t = [\overrightarrow{h_t} : \overleftarrow{h_t}]$ concatenates the forward LSTM unit $\overrightarrow{h_t}$ and backward LSTM unit $\overleftarrow{h_t}$ to obtain the characteristic representation of the long-range interaction information between the amino acids *k*-mers.

The output of the LSTM layer is flattened to a one-dimensional array and then fed into a fully connected layer with 256 hidden neurons using a ReLU activation function. Finally, the prediction score is generated by a fully connected output layer with a softmax activation function:

$$\sigma(z)_j = \frac{e^{z_j}}{e^{z_1} + e^{z_2}},$$

where $\sigma(z)_j$ is the probability value of the *j*th element.

2.3 Model training

We use 10-fold cross-validation to train 10 models, respectively. The protein sequences are randomly divided into ten disjoint parts. Alternatively, nine parts serve the purpose of training and the rest is used for validation. The final results are reported by taking advantage of the ten models. The Adam (Adaptive moment estimation) optimizer (Kingma and Ba, 2014) is adopted for model training. Validation sets are used to allow early stop during training to prevent the network from overfitting. It is important to note that there are approximately five times more uncrystallizable proteins than the crystallizable proteins in our training set, which leads to an imbalance training problem. To address this issue, in the training of each fold, we randomly down sample all negative sequences to the number approximately the same as the positive ones. The negative sequence down sampling step is repeated in each epoch.

CLPred is implemented using Google's open source TensorFlow library (Abadi *et al.*, 2016). To speed up the training, we use the GPU version of TensorFlow to train on the Nvidia Titan X GPU.

2.4 Evaluation strategies

We use multiple evaluation indicators including the area under the curve (AUC), accuracy (ACC), Recall (REC), Precision (PRE), F-score, NPV, and Matthews correlation coefficient (MCC) (Matthews, 1975) as the measures to evaluate the predictive performances of the protein crystallization predictors. The AUC value quantifies the area under the receiver operating characteristic curve (ROC) by plotting the true-positive rates against the false-positive rates. Matthews Correlation Coefficient (MCC) takes true positive (TP), true negative (TN), false positive (FP), and false negative (FN) into account. The evaluation indicators used in the paper are summarized as follows:

$$\mathrm{MCC} = \frac{(\mathrm{TP} \times \mathrm{TN} - \mathrm{FP} \times \mathrm{FN})}{\sqrt{(\mathrm{TP}+\mathrm{FP}) \times (\mathrm{TP}+\mathrm{FN}) \times (\mathrm{TN}+\mathrm{FP}) \times (\mathrm{TN}+\mathrm{FN})}}$$

$$\mathrm{ACC} = \frac{(\mathrm{TP}+\mathrm{TN})}{(\mathrm{TP}+\mathrm{TN}+\mathrm{FP}+\mathrm{FN})}$$

$$\mathrm{REC} = \frac{\mathrm{TP}}{(\mathrm{TP}+\mathrm{FN})}, \mathrm{PRE} = \frac{\mathrm{TP}}{(\mathrm{TP}+\mathrm{FP})}$$

$$\mathrm{F-score} = \frac{2 * \mathrm{REC} * \mathrm{PRE}}{(\mathrm{REC}+\mathrm{PRE})}$$

$$\mathrm{NPV} = \frac{\mathrm{TN}}{\mathrm{TN}+\mathrm{FN}}$$

3 Results and Discussions

3.1 Performance of the CLPred on three benchmark data sets

We evaluate the predictive performances of five sequence-based protein crystallization predictors, including DETECT, TargetCrys, PPCPred, CrystalP2, and DeepCrystal. The prediction results on DC_final, SP_final, and TR_final are shown in Tables 2, 3, and 4, respectively. One can find that CLPred outperforms the predictors when performance is measured by Accuracy, AUC, Recall, F-score, NPV, and MCC. When measured by prediction precision, CLPred is slightly inferior to DeepCrystal, fDETECT, and DeepCrystal/fDETECT in DC_final, SP_final, and TR_final, respectively. However, the gains of CLPred measured by the other metrics are more significant. ROC curves for the five predictors of the three different test sets are shown in Fig. 2.

Table 2. Performance comparison of the available predictors evaluated on the DC_final data set.

Method	Accuracy	AUC	Precision	Recall	F-score	NPV	MCC
fDETECT	0.650	0.782	0.841	0.367	0.597	0.597	0.360
TargetCrys	0.628	0.638	0.620	0.653	0.636	0.636	0.256
PPCPred	0.672	0.754	0.740	0.528	0.616	0.635	0.359
CrystalP2	0.586	0.607	0.570	0.696	0.627	0.612	0.178
DeepCrystal	0.799	0.915	**0.885**	0.685	0.772	0.744	0.613
CLPred	**0.851**	**0.928**	0.849	**0.852**	**0.850**	**0.852**	**0.700**

Note: Bold represents best results

Table 3. Performance comparison of the available predictors evaluated on the SP_final data set.

Method	Accuracy	AUC	Precision	Recall	F-score	NPV	MCC
fDETECT	0.616	0.837	**0.913**	0.426	0.581	0.494	0.382
TargetCrys	0.608	0.642	0.727	0.595	0.654	0.483	0.217
PPCPred	0.666	0.784	0.863	0.554	0.675	0.535	0.403
CrystalP2	0.654	0.697	0.711	0.750	0.730	0.543	0.249
DeepCrystal	0.683	0.866	0.910	0.547	0.684	0.547	0.457
CLPred	**0.801**	**0.887**	0.885	**0.783**	**0.832**	**0.698**	**0.599**

Table 4. Performance comparison of the available predictors evaluated on the TR_final data set.

Method	Accuracy	AUC	Precision	Recall	F-score	NPV	MCC
fDETECT	0.750	0.848	0.823	0.411	0.548	0.733	0.447
TargetCrys	0.634	0.693	0.503	0.788	0.614	0.814	0.325
PPCPred	0.748	0.819	0.677	0.606	0.640	0.782	0.448
CrystalP2	0.581	0.673	0.460	0.775	0.577	0.78	0.241
DeepCrystal	0.803	0.914	**0.838**	0.580	0.686	0.792	0.569
CLPred	**0.854**	**0.930**	0.787	**0.829**	**0.807**	**0.896**	**0.690**

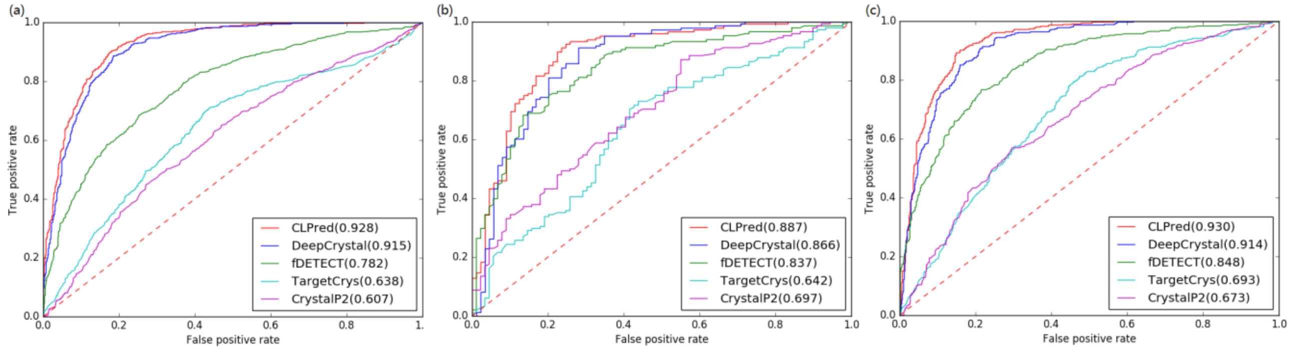

Fig. 2. ROC curves for the five predictors of the three different test sets. (a) ROC curve for DC_final, (b) ROC curve for SP_final data set and (c) ROC curve for TR_final dataset. The AUC values of the five predictors are shown in the figure legend.

3.2 Model analysis

The advantage of using deep learning for protein crystallization is that the neural networks can have multiple layers, each of which learns to detect and select hierarchical features of a sequence. This starts from simple features, such as local *k*-mers conformations and properties, and gradually increases in complexity to features, such as long-range, high-order *k*-mers interactions, that uniquely characterize a protein. Here, we project the feature vectors derived from each layer in the CLPred model to a two-dimensional feature space via t-SNE (Maaten and Hinton, 2008), principle component analysis (PCA), and UMAP (McInnes *et al.*, 2018), and visualize the overall process of protein crystallization classification in Fig. 3. We extract five features vectors from the embedding layer, the pooling layer after the first CNN layer, the pooling layer after the second CNN layer, the BLSTM layer, and the fully connected layer. As shown in Fig. 3(a-e), one can observe that, as the layers deepen in CLPred, the feature vectors learned become gradually more effective in distinguishing crystallizable proteins from the non-crystallizable ones. In particular, the features from the embedding layer mainly characterize the local features of *k*-mers, which do not contribute much in separating the two classes. However, as the CNN, pooling, and BLSTM layers derive and select more complex features representing high-order, global *k*-mers interactions, the crystallizable proteins and non-crystallizable proteins become more separable.

In Table 5, we compare different CLPred architectures with different hyperparameters and layers. Our current architecture with two convolution layers, one BLSTM layer, and one fully-connected layer yields the optimal prediction capability. Adding additional convolution layers or fully connected layers not only increases the computational cost, but also downgrades the prediction performance.

Table 5. Performance comparison of different CLPred architectures on the DC_final data set for 10-fold cross-validation.

Method	Accuracy
E	0.752
E+MSCNN_8	0.799
E+MSCNN_8+MSCNN_3	0.821
E+MSCNN_8+MSCNN_3+BLSTM	0.845
E+MSCNN_8+MSCNN_3+BLSTM+FC_256	0.850
E+MSCNN_8+MSCNN_3+BLSTM+CNN_3+CNN_3+CNN_3	0.847
E+MSCNN_8+MSCNN_3+BLSTM+CNN_3+CNN_3+CNN_3+FC_256	0.849
E+MSCNN_8+MSCNN_3+BLSTM+CNN_3+CNN_3+CNN_3+FC_1024+FC_256	0.848

E: embedding layer, MSCNN_8: multi-scale convolution layer, the convolution kernel size of each scale is {2, 3, 4, 5, 6, 7, 8, 9}, MSCNN_3: multi-scale convolution layer, the convolution kernel size of each scale is {5, 9, 13}, BLSTM: three-layer bidirectional long short-term memory neural network, CNN_3: convolution layer, whose convolution kernel size is 3, followed by average pooling with a sliding window of length 5 and step length 1, FC_1024: fully connected layer with 1024 neurons, FC_256: fully connected layer with 256 neurons.

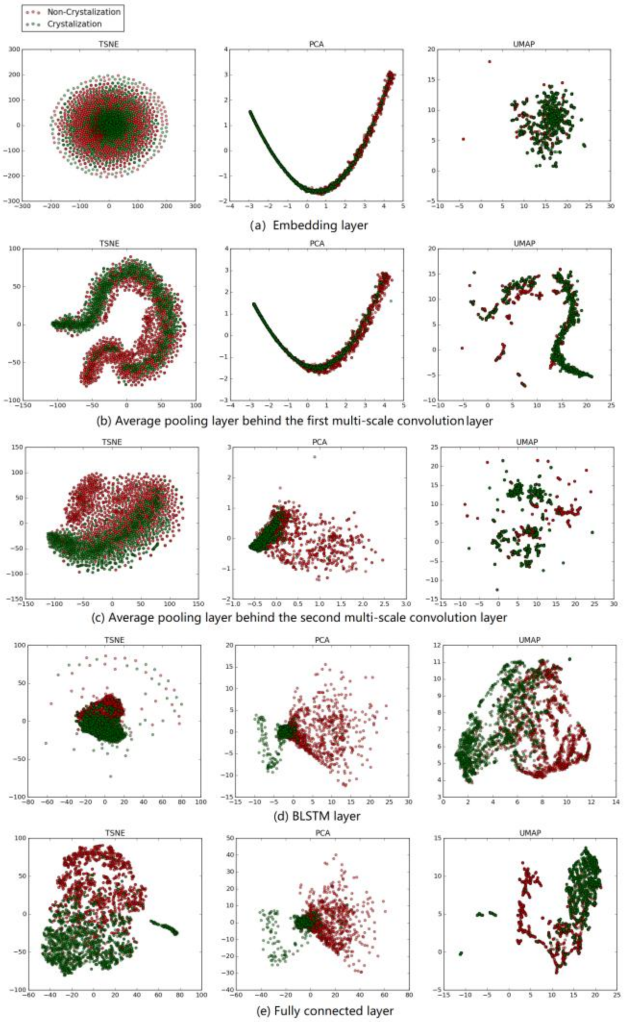

(a) Embedding layer

(b) Average pooling layer behind the first multi-scale convolution layer

(c) Average pooling layer behind the second multi-scale convolution layer

(d) BLSTM layer

(e) Fully connected layer

Fig. 3. The feature vectors of the three test sets in the five hidden layers are visualized after dimensionality reduction by t-SNE, PCA and UMAP. The red circle represents the non-crystallizable sequence and the blue circle represents the crystallizable ones. (a) feature vectors in the embedding layer. (b) feature vectors of the first average pooling layer. (c) feature vectors of the second pooling layer. (d) feature vectors of the BLSTM layer. (e) feature vectors from the final fully connected layer.

Table 6. The numbers of amino acids corresponding to the top five and ten activation values across all samples.

Amino acid	Top 5 (rank)	Top 10 (rank)	Amino acid	Top 5 (rank)	Top 10 (rank)
R-Arg	84316(1)	153966(1)	T-Thr	11844(11)	26653(11)
I-Ile	83155(2)	151492(2)	L-Leu	9204(14)	22481(12)
Q-Gln	41350(3)	77743(3)	M-Met	10465(12)	22344(13)
G-Gly	22039(6)	49354(4)	N-Asn	9198(15)	20732(14)
S-Ser	22097(5)	46728(5)	E-Glu	7807(17)	19164(15)
V-Val	19970(7)	44854(6)	H-His	8736(16)	19037(16)
C-Cys	22760(4)	40599(7)	W-Trp	9279(13)	18640(17)
Y-Tyr	18295(8)	36675(8)	K-Lys	6057(18)	14612(18)
F-Phe	15533(9)	32412(9)	D-Asp	3972(19)	9989(19)
P-Pro	12957(10)	29158(10)	A-Ala	1152(20)	3487(20)

Table 7. The numbers of tripeptides corresponding to the top five and ten activation values across all samples.

Tripeptides	Top 10	Tripeptides	Top 5
RRR	1812	III	1399
III	1733	RRR	1383
IIS	1279	IIS	848
RII	1141	RII	833
RRI	1055	RRI	695
IIG	978	QRR	627
RVR	943	RIR	620
LII	938	RVR	613
RIR	926	RQR	609
IIF	887	IIR	582
IFI	868	IFI	573
RQR	848	IIF	571
IIV	841	RRQ	570
QRR	828	QII	556
SII	825	IIG	536
IIR	823	LII	518
RRV	811	IRR	503
FII	792	RRV	489
QII	791	RSR	487
IRR	790	SII	481

3.3 Key amino acids and tripeptides related to protein crystallization

We take the 800x64 feature map generated by the first multi-scale convolution, average the data of the second dimension, and normalize them to [0, 1]. Then, each sequence is represented by a vector of length 800 and each value in this vector is the activation value corresponding to the amino acid in the sequence. The larger the activation values of amino acid, the greater its contribution to the classification results. According to the activation values, we summarize the total numbers of amino acids in Table 6. The top seven amino acids that mostly contribute to protein crystallization are R(Arg), I(Ile), Q(Gln), G(Gly), V(Vla), S(Ser) and C(Cys). This is generally consistent with the results presented in Charoenkwan et al. (2013) while our results indicate that R(Arg) and I(Ile) are also important to protein crystallization.

In addition to the contribution of an individual amino acid, the feature vector extracted from the CNN layer with a kernel size of 3 allows us to gain insight in more specific contributions of tripeptides. By applying similar counting as single amino acids, the top-ranked triplets are derived and shown in Table 7. It is interesting to note that most of these tripeptides include R(Arg) and/or I(Ile). This indicates that the tripeptides heavily involved R(Arg) and/or I(Ile) play an important role in protein crystallization process. Their mechanism deserves further computational and experimental studies.

3.4 Effectiveness of BLSTM

The BLSTM layer is a crucial component in CLPred for capturing the high-order, long-range *k*-mers interactions. In order to demonstrate the effectiveness of BLSTM, we compare the prediction performance of CLPred with a CLPred version by replacing the BLSTM layer with a CNN layer. We name this CLPred_noBLSTM. Notice that CLPred_noBLSTM has a similar architecture as DeepCrystal. The 10-fold cross-validation results of CLPred, CLPred_noBLSTM, and DeepCrystal on DC_final, SP_final, and TR_final are shown in Table 8, respectively. One can find that CLPred_noBLSTM and DeepCrystal differ only 0.1%~2% for most of the metrics, but CLPred with BLSTM is significantly higher in comparison. This confirms that the feature representation learned by BLSTM plays an important role in effectively predicting which sequences can produce diffraction-quality crystals.

Table 8. Verify the effectiveness of the BLSTM on three benchmark data sets (Bold represents best results).

Model	ACC	AUC	PRE	REC	F-score	NPV	MCC
DC_final							
DeepCrystal	0.799	0.915	**0.885**	0.685	0.772	0.744	0.613
CLPred_noBLSTM	0.815	0.911	0.862	0.750	0.802	0.780	0.636
CLPred	**0.851**	**0.928**	0.849	**0.852**	**0.85**	**0.852**	**0.700**
SP_final							
DeepCrystal	0.683	0.866	**0.910**	0.547	0.684	0.547	0.457
CLPred_noBLSTM	0.722	0.879	0.890	0.628	0.738	0.586	0.493
CLPred	**0.801**	**0.887**	0.885	**0.783**	**0.832**	**0.698**	**0.599**
TR_final							
DeepCrystal	0.803	0.914	**0.838**	0.580	0.686	0.792	0.569
CLPred_noBLSTM	0.816	0.907	0.796	0.676	0.731	0.826	0.597
CLPred	**0.854**	**0.930**	0.787	**0.829**	**0.807**	**0.896**	**0.690**

Table 9. Performance comparison between CLPred, BCrystal, and CLPred_AF, which combines the last layer features of CLPred with 641 additional features.

Method	ACC	AUC	PRE	REC	F-score	NPV	MCC
DC_final							
CLPred	0.851	0.928	0.849	0.852	0.850	0.852	0.700
BCrystal	0.954	0.979	0.938	**0.973**	0.955	**0.972**	0.910
CLPred_AF	**0.957**	**0.987**	**0.945**	0.970	**0.957**	0.969	**0.914**
TR_final							
CLPred	0.854	0.930	0.787	0.829	0.807	0.896	0.690
BCrystal	0.964	0.987	0.931	**0.976**	0.953	**0.985**	0.925
CLPred_AF	**0.968**	**0.993**	**0.945**	0.971	**0.958**	0.982	**0.933**
SP_final							
CLPred	0.801	0.887	0.885	0.783	0.832	0.698	0.599
BCrystal	0.903	0.948	0.888	**0.966**	0.926	**0.934**	0.793
CLPred_AF	**0.911**	**0.971**	**0.904**	0.960	**0.931**	0.925	**0.810**

3.5 Additional features other than sequence

Crystallization prediction can be further improved when additional features, such as evolutionary information and predicted protein properties such as secondary structure, flexibility, structural motif, solvent accessibility, and disulfide bond, are incorporated. Recently, BCrystal (Elbasir *et al.*, 2020) uses pre-extracted evolutional, structural, and physicochemical characteristics as additional features and employs XGBoost (Chen and Guestrin, 2016) to predict protein crystallization propensity, which has shown significant performance enhancement. These features can also be used in the CLPred framework. Table 9 shows the performance comparison between CLPred, BCrystal, and CLPred_AF, which combines the last layer features of CLPred with 641 additional features, including 8-state secondary structure (SS), fraction of exposed residues (FER), disorder, and hydrophobicity. These features are obtained from Elbasir *et al.* (2020). One can find that, when these additional features are incorporated, the performance of CLPred_AF is also significantly improved compared to CLPred and is at least comparable to BCrystal. Nevertheless, CLPred, as predictor using sequence-only features, is still of practical use, since it does not rely on the accuracy of other feature prediction tools and is not biased to the databases of deriving additional features.

3.6 Analysis the impact of sequence identity cutoff

In data preprocessing, most studies remove sequences with over 25% sequence identity in the training set (Wang et al. 2014; Wang et al. 2018; Elbasir et al. 2019). While 25% cutoff may still lead to homologues with recognizable alignments, we hereby compare the performance of CLPred models trained with lower sequence identity cutoffs. As shown in Table 10, the prediction results on the test sets for datasets under 15%, 20%, and 25% sequence identity cutoffs are rather consistent, although lowering sequence identity cutoffs results in training sets with reduced sizes. This indicates that 25% is a reasonable sequence identity cutoff to benchmark CLPred and compare it with other crystallization prediction methods.

Table 10. Compare the performance of CLPred models in test sets with different cutoff sequence identity.

Cutoff	ACC	AUC	PRE	REC	F-score	NPV	MCC
DC_final							
25%	0.851	0.928	0.849	0.852	0.850	0.852	0.700
20%	0.850	0.927	0.864	0.829	0.847	0.837	0.700
15%	0.843	0.926	0.863	0.814	0.837	0.825	0.687
SP_final							
25%	0.801	0.887	0.885	0.783	0.832	0.698	0.599
20%	0.793	0.888	0.909	0.743	0.817	0.672	0.600
15%	0.785	0.890	0.900	0.736	0.810	0.664	0.582
TR_final							
25%	0.854	0.930	0.787	0.829	0.807	0.896	0.690
20%	0.852	0.924	0.808	0.787	0.797	0.877	0.680
15%	0.852	0.927	0.815	0.778	0.796	0.873	0.681

4 Cases analysis

4.1 Sox transcription factors analysis

Sox proteins are sequence-specific transcription factors that regulate several key developmental processes. It contains a highly conserved high-mobility group (HMG) domain of ~80 amino acids, known for binding and bending the DNA (Vivekanandan *et al.*, 2015). Sox17 and Sox9 are members of the Sox transcription factor family. Sox17 is involved in endodermal differentiation during early mammalian development. Sox9 is a fundamental sex-determining gene involved in the development of various vital organs, such as testicles, kidneys, heart, and brain, and skeletal development. We use CLPred to predict several Sox proteins such as the full-length Sox17, full-length Sox9, Sox17 HMG domain, Sox9 HMG domain, and Sox17 mutant (EK) HMG domain collected by Elbasir *et al.* (2019) and compare with the other sequence-based protein crystal predictors. The results are listed in Table 11. Recent studies have shown that Sox9 HMG, Sox17 HMG and Sox17EK HMG can produce diffraction-quality crystals (Palasingam *et al.*, 2009; Vivekanandan *et al.*, 2015; Elbasir *et al.*, 2019). In addition, there is no evidence to show that full-length sequences of Sox9 and Sox17 can produce diffraction-quality crystals. The results in Table 11 show that CLPred and DeepCrystal are the only two methods that can correctly identify Sox9 HMG, Sox17 HMG, and Sox17EK HMG as the ones that can produce diffraction-quality crystals. It is worthy to note that the score of CLPred is much higher than the other predictors. For those having no evidence of producing diffraction-quality crystals, all sequence-based protein crystallization tools, including CLPred, make the same predictions which are uncrystallizable. This indicates that both full-length sequences of Sox9 and Sox17 are unlikely to produce diffraction-quality crystals in industrial production.

Table 11. Prediction scores of the CLPred and other predictors for some Sox transcription factor family protein.

	Sox9 Full Length	Sox9 HMG	Sox17 Full Length	Sox17 HMG	Sox17 EK HMG
CLPred	0.155	0.886	0.235	0.858	0.872
DeepCrystal	0.315	0.676	0.430	0.643	0.633
fDETECT	0.070	0.432	0.075	0.462	0.418
TargetCrys	0.032	0.045	0.037	0.029	0.031
PPCPred	0.039	0.658	0.089	0.462	0.523
CrystalP2	0.327	0.459	0.470	0.436	0.402

4.2 Zika virus proteins analysis

Zika virus is a plus single-stranded RNA virus, a member of the flavivirus genus of the Flaviviridae, and its genome encodes three structural proteins (nucleocapsid protein C, membrane protein M, and envelope protein E) and seven non-structural proteins (NS1, NS2A, NS2B, NS3, NS4A, NS4B, and NS5). We have collected some crystallizable Zika protein sequences, including full-length NS1 (Brown *et al.*, 2016), C-terminal fragment of NS1 (Song *et al.*, 2016), unlinked NS2B-NS3 protease in complex with a compound fragment (Zhang *et al.*, 2016), NS2B-NS3 protease in complex with a boronate inhibitor (Lei *et al.*, 2016), and NS5 methyltransferase in complex with GTP and SAH (Zhang *et al.*, 2017). We have also tested some other non-structural proteins, where no evidence shows that they can produce diffraction-quality crystals so far, like the full-length protein sequences of NS2A, NS2B, NS4A, and NS4B. Determining the structures of these important non-structural proteins will lay a significant foundation to understand and overcome the Zika virus.

Table 12. Prediction scores of the CLPred and other predictors for some Zika virus non-structural proteins

Protein	CLPred	DeepCrystal	fDETECT	TargetCrys	PPCPred	CrystalP2
NS1 FL	0.997	0.472	0.157	0.084	0.233	0.57
NS1[1]	0.717	0.667	0.224	0.030	0.257	0.534
NS2B-NS3[2]	0.686	0.680	0.456	0.137	0.320	0.645
NS2B-NS3[3]	0.827	0.808	0.925	0.563	0.961	0.581
NS5[4]	0.865	0.494	0.274	0.030	0.215	0.375
NS2A FL	0.001	0.140	0.629	0.075	0.307	0.454
NS2B FL	0.636	0.626	0.594	0.145	0.585	0.577
NS4A FL	0.338	0.425	0.536	0.123	0.364	0.701
NS4B FL	0.028	0.066	0.015	0.097	0.302	0.468

NS1[1]：C-terminal fragment of NS1. NS2B-NS3[2]：NS2B-NS3 protease in complex with a boronate inhibitor. S2B-NS3[3]：Unlinked NS2B-NS3 protease from Zika virus in complex with a compound fragment. NS5[4]：NS5 methyltransferase in complex with GTP and SAH. FL: Full Length

We use CLPred to predict these proteins and compare them with the sequence-based protein crystal predictors. The results are provided in Table 12. As shown in Table 12, CLPred is the only model that 100% correctly identifies the non-structural Zika virus proteins which can produce diffraction-quality crystals. For non-structural full-length proteins NS2A, NS2B, and NS4A with uncertain labels, crystallization propensity predicted by CLPred is consistent with the predictions generated by most of the other predictors. For full-length NS4B, the predicted score of CLPred is 0.028, which is also consistent with other predictors. In addition, we observe that full-length NS2B is predicted with relatively high confidence by CLPred and four other tools, which deserves further investigation by the Zika virus research community.

5 Conclusions and Future Work

To avoid time-consuming and expensive experimentations with proteins that are not likely to result in resolvable crystallized structures, the selection of targets for structure determination is one of the greatest challenges in structural genomics experiments (Varga *et al.*, 2017). In this study, we propose CLPred, a sequence-based deep learning framework. Using only information from sequence, CLPred employs a BLSTM in its deep learning architecture to capture the high-order, long-range interaction patterns between *k*-mers, which makes up the deficiency of the previous work using CNN. It has been steadily improved over the previous window-based neural networks and is able to predict the crystallization propensity with higher accuracy. This performance enhancement is due to the ability of BLSTM to recognize non-local interactions, as using the local interaction features has already reached its limit in traditional neural networks. Cross-validation and independent tests on three benchmark data sets and ablation study have confirmed the efficacy of BLSTM in protein crystallization prediction where non-local interactions are crucial. By analyzing the feature vectors derived from various layers in CLPred architecture, we have found the key amino acids and tripeptides mostly contributing to protein crystallization. By combining the last layer features of CLPred with 641 additional features, we obtain the improving performance, which is at least comparable to that of BCrystal. Finally, the correctness of our CLPred predictions is further validated by the case studies of Sox transcription factor family member proteins and Zika virus non-structural proteins. Our future work will be analyzing and interpreting the patterns learned in CLPred via deep learning and understanding the fundamentals governing protein crystallization.

CLPred is freely available and downloadable at GitHub: https://github.com/xuanwenjing/CLPred.

Fundings

This work is supported in part by the NSFC-Zhejiang Joint Fund for the Integration of Industrialization and Informatization under grant (No. U1909208), National Natural Science Foundation of China under grant (No. 61832019), 111 Project (No. B18059) and Hunan Provincial Science and Technology Program (No. 2018WK4001).

Conflict of Interest: none declared.

References

Bethel C. M., Lieberman R. L. (2014) Protein structure and function: An interdisciplinary multimedia-based guided-inquiry education module for the high school science classroom. *J.Chem. Educ.*, **91**, 52-55.

Xue Y. *et al.* (2013) Efficacy and safety of computer-assisted stereotactic transplantation of human retinal pigment epithelium cells in the treatment of Parkinson disease. *J. Comput. Tomogr.*, **37**, 333-337.

Chen C., Yu C. (2013) A novel integrated framework and improved methodology of computer-aided drug design. *Curr. Top. Med. Chem.*, **13**, 965-988.

Cordeiro M. N., Speck-Planche A. (2012) Computer-aided drug design, synthesis and evaluation of new anti-cancer drugs. *Curr. Top. Med. Chem.*, **12**, 2703-2704.

Service R. (2005) Structural biology. Structural genomics, round 2. *Science*, **307**, 1554.

Kurgan L., Mizianty M. J. (2009) Sequence-based protein crystallization propensity prediction for structural genomics: review and comparative analysis. *Natural Science*, **1**, 93.

Slabinski L. *et al.* (2007) The challenge of protein structure determination-lessons from structural genomics. *Protein Science*, **16**, 2472-2482.

Jahandideh S. *et al.* (2014) Improving the chances of successful protein structure determination with a random forest classifier. *Acta Crystallogr. D Biol.*, **70**, 627-635.

Sánchez-Puig N. *et al.* (2012) Predicting protein crystallizability and nucleation. *Protein Pept. Lett.*, **19**, 725-731.

Canaves J. M. *et al.* (2004) Protein biophysical properties that correlate with crystallization success in Thermotoga maritima: maximum clustering strategy for structural genomics. *J. Mol. Biol.*, **344**, 977-991.

Goh C. S. *et al.* (2004) Mining the structural genomics pipeline: identification of protein properties that affect high-throughput experimental analysis. *J. Mol. Biol.*, **336**, 115-130.

Kurgan L. *et al.* (2009) CRYSTALP2: sequence-based protein crystallization propensity prediction. *BMC Struct. Biol.*, **9**, 50.

Chen K. *et al.* (2007) Prediction of protein crystallization using collocation of amino acid pairs. *Biochem. Bioph. Res. Co.*, **355**, 764-769.

Mizianty M. J., Kurgan L. (2011) Sequence-based prediction of protein crystallization, purification and production propensity. *Bioinformatics*, **27**, i24-i33.

Wang H. *et al.* (2014) PredPPCrys: accurate prediction of sequence cloning, protein production, purification and crystallization propensity from protein sequences using multi-step heterogeneous feature fusion and selection. *PLoS One*, **9**, e105902.

Jahandideh S. *et al.* (2014) Improving the chances of successful protein structure determination with a random forest classifier. *Acta Crystallogr. D Biol.*, **70**, 627-635.

Slabinski L. *et al.* (2007) XtalPred: a web server for prediction of protein crystallizability. *Bioinformatics*, **23**, 3403-3405.

Hu J. *et al.* (2016) TargetCrys: protein crystallization prediction by fusing multi-view features with two-layered SVM. *Amino acids*, **48**, 2533-2547.

Wang H. *et al.* (2018) Critical evaluation of bioinformatics tools for the prediction of protein crystallization propensity. *Brief. Bioinform.*, **19**, 838-852.

Meng F. *et al.* (2017) fDETECT webserver: fast predictor of propensity for protein production, purification, and crystallization. *BMC bioinformatics*, **18**, 580.

Elbasir A. *et al.* (2019) DeepCrystal: a deep learning framework for sequence-based protein crystallization prediction. *Bioinformatics*, **35**, 2216-2225.

LeCun Y. *et al.* (1998) Gradient-based learning applied to document recognition. *P. IEEE*, **86**, 2278-2324.

Szegedy C. *et al.* (2015) Going deeper with convolutions. In: *Proc. IEEE Conf. Comp. Vision Patt. Recog.*, pp. 1-9.

Hochreiter S., Schmidhuber J. (1997) Long short-term memory. *Neural Comput.*, **9**, 1735-1780.

Sutskever I. *et al.* (2014) Sequence to sequence learning with neural networks. In: *Proc. Adv. Neural Inf. Process. Syst.*, pp. 3104-3112.

Graves A., Jaitly N. (2014) Towards end-to-end speech recognition with recurrent neural networks. In: *Int. Conf. Mach. Learn.*, pp. 1764-1772.

Sønderby S. K., Winther O. (2014) Protein secondary structure prediction with long short term memory networks. *arXiv*, **1412**, 7828.

Fu L. *et al.* (2012) CD-HIT: accelerated for clustering the next-generation sequencing data. *Bioinformatics*, **28**, 3150-3152.

Elbasir A. *et al.* (2020) BCrystal: an interpretable sequence-based protein crystallization predictor. *Bioinformatics*, **36**, 1429-1438

Kouranov A. *et al.* (2006) The RCSB PDB information portal for structural genomics. *Nucleic Acids Res.*, **34**(suppl. 1), D302-D305.

Gräslund S. *et al.* (2008) Protein production and purification. *Nature methods*, **5**, 135.

Vang Y. S., Xie X. (2017) HLA class I binding prediction via convolutional neural networks. *Bioinformatics*, **33**, 2658-2665.

Nair V., Hinton G. E. (2010) Rectified linear units improve restricted boltzmann machines. In: *Proc., Int. Conf. Mach. Learn.*, pp. 807-814.

Krizhevsky A. *et al.* (2012) Imagenet classification with deep convolutional neural networks. In: *Proc. Adv. Neural Inf. Process. Syst.*, pp. 1097-1105.

LeCun Y. *et al.* (2015) Deep learning. *nature*, **521**, 436-444.

Hinton G. E. *et al.* (2012) Improving neural networks by preventing co-adaptation of feature detectors. *arXiv* , **1207**, 0580.

Kingma D. P., Ba J. (2014) Adam: A method for stochastic optimization. *arXiv* ,**1412**, 6980.

Abadi M. *et al.* (2016) Tensorflow: Large-scale machine learning on heterogeneous distributed systems. *arXiv*, **1603**, 04467.

Matthews B. W. (1975) Comparison of the predicted and observed secondary structure of T4 phage lysozyme. *BBA-Protein Struct.*, **405**, 442-451.

Maaten L., Hinton G. (2008) Visualizing data using t-SNE. *J. Mach. Learn. Res.*, **9**, 2579-2605.

McInnes L. *et al.* (2018) Umap: Uniform manifold approximation and projection for dimension reduction. *arXiv* , **1802**, 03426.

Charoenkwan P. *et al.* (2013) SCMCRYS: predicting protein crystallization using an ensemble scoring card method with estimating propensity scores of P-collocated amino acid pairs. *PloS one*, **8**, e72368.

Vivekanandan S. *et al.* (2015) Crystallization and X-ray diffraction analysis of the HMG domain of the chondrogenesis master regulator Sox9 in complex with a ChIP-Seq-identified DNA element. *Acta Crystallogr. F Struct. Biol. Commun.*, **71**, 1437-1441.

Palasingam P. *et al.* (2009) The structure of Sox17 bound to DNA reveals a conserved bending topology but selective protein interaction platforms. *J. Mol. Biol.*, **388**, 619-630.

Brown W. C. *et al.* (2016) Extended surface for membrane association in Zika virus NS1 structure. *Nat. Struct. Mol. Biol.*, **23**, 865-867.

Song H. *et al.* (2016) Zika virus NS1 structure reveals diversity of electrostatic surfaces among flaviviruses. *Nat. Struct. Mol. Biol.*, **23**, 456.

Lei J. *et al.* (2016) Crystal structure of Zika virus NS2B-NS3 protease in complex with a boronate inhibitor. *Science*, **353**, 503-505.

Zhang Z. *et al.* (2016) Crystal structure of unlinked NS2B-NS3 protease from Zika virus. *Science*, **354**, 1597-1600.

Zhang C. *et al.* (2017) Structure of the NS5 methyltransferase from Zika virus and implications in inhibitor design. *Biochem. Biophys. Res. Commun.*, **492**, 624-630.

Varga J. *et al.* (2017) TSTMP: target selection for structural genomics of human transmembrane proteins. *Nucleic Acids Res.*, **45**, D325-D330.

Li Y. *et al.* (2011) Sampling multiple scoring functions can improve protein loop structure prediction accuracy. *J. Chem. Inf. Model.*, **51**, 1656-1666.

Elhefnawy W. *et al.* (2019) Decoding the Structural Keywords in Protein Structure Universe. *J. Comput. Sci. Technol.*, **34**, 3-15.

Chen T., Guestrin C. (2016) Xgboost: A scalable tree boosting system. In: *Proc. 22th ACM SIGKDD Int Conf Knowl. Discovery Data Mining*, pp. 785-794.